

Electric Field Induced Sphere-to-Cylinder Transition in Diblock Copolymer Thin Films

Ting Xu,[†] A. V. Zvelindovsky,[‡] G. J. A. Sevink,[‡] Oleg Gang,[§] Ben Ocko,[§]
Yuqing Zhu,[†] Samuel P. Gido,[†] and Thomas P. Russell^{*,†}

Department of Polymer Science and Engineering, University of Massachusetts,
Amherst, Massachusetts 01003, Leiden Institute of Chemistry, Leiden University,
P.O. Box 9502, 2300 RA Leiden, The Netherlands, and Department of Physics,
Brookhaven National Laboratory, Upton, New York 11973

Received April 20, 2004; Revised Manuscript Received June 21, 2004

ABSTRACT: An electric field induced sphere-to-cylinder transition in thin films of asymmetric polystyrene-*b*-poly(methyl methacrylate) diblock copolymers was observed. In the absence of an applied electric field, thin films of the asymmetric diblock copolymer consisted of layers of spherical microdomains with poor in-plane long-range ordering. Under a $\sim 40\text{V}/\mu\text{m}$ applied electric field, hexagonally packed cylindrical microdomains normal to the surface were found. Cross-sectional transmission electron microscopy images of the intermediate stages of the alignment indicated that, under an electric field, the asymmetric diblock copolymer formed spherical microdomains that were deformed into ellipsoids and, with time, interconnected into cylindrical microdomains oriented in the direction of the applied electric field. Simulations suggest that improved long-range order of the cylindrical microdomains could be achieved by cycling the electrical field.

Introduction

Diblock copolymers are composed of chemically different polymers covalently coupled at one end that microphase separate into morphologies ranging from spheres to cylinders to lamellae (and other morphologies) depending on the volume fraction of each block and χN , where χ is the Flory–Huggins segmental interaction parameter and N is the degree of polymerization.^{1,2} In general, χ is inversely proportional to the temperature. By increasing temperature, χN decreases and transitions between different morphologies, called order-to-order transitions (OOT), occur. Thermoreversible OOTs in the weak segregation limit were theoretically predicted years ago.³ Experimentally, different transitions, such as cylinder to gyroid and sphere to cylinder, have been reported in bulk copolymer systems.^{4–12} For example, Sakurai et al. reported the thermoreversible OOT between spheres in a body-centered cubic lattice to hexagonal cylinders for a polystyrene-*b*-polyisoprene diblock copolymer. The cylinders were transformed into a series of spheres, where the axes of the cylinders defined the [111] direction of the bcc-spheres upon heating. The spheres deformed and interconnected forming cylinders upon cooling.

Electric fields have been shown as an effective method of controlling copolymer microdomains orientation.^{13–17} Experimental results and theoretical calculations show that the electric field enhances fluctuations along the interface between two blocks because of the difference in dielectric constants of the microdomains and aligns the microdomains in the direction of the applied field to lower the free energy.^{18–20} Numerous studies have described the mechanism by which the electric field reorients the anisotropic microdomains.^{21–25} However,

it should also be possible to induce an OOT, such as the sphere-to-cylinder transition, with an applied field.

It is well known that a spherical dielectric can be deformed into an ellipsoid under the influence of an applied electric field.²⁶ Recently, Tsori et al. suggested that the presence of dissociated ions in block copolymers, as opposed to simply a difference in the dielectric constants, can be used to induce morphological changes under an electric field and lead to phase transitions.²⁷ Under sufficiently high electric fields, it should be possible to deform spherical microdomains into ellipsoids and, for a thin block copolymer film with multiple layers of spheres, the ellipsoids can be sufficiently stretched such that they interconnect to form cylinders that penetrate through the film. Conservation of volume requires that the diameters of the cylinders be smaller than those of the spherical microdomains. Such a sphere-to-cylinder transition may offer a simple route to generate cylinders with high aspect ratios from spherical microdomains. As shown by Kramer et al. and Register et al., it is possible to generate thin films with exceptional long-range order using block copolymers with spherical microdomains. Thus, by using a sphere-to-cylinder transition, a simple route to achieve highly ordered arrays of nanoscopic cylindrical domains having large aspect ratio may be possible.^{28,29}

Experimental

Here, we report on an electric field induced sphere-to-cylinder transition in diblock copolymer thin films of a polystyrene-*b*-poly(methyl methacrylate) diblock, denoted as PS-*b*-PMMA. PS-*b*-PMMA was prepared by anionic synthesis having a molecular weight of 151 000 g/mol, a polydispersity of 1.06, and a PS volume fraction of 0.9, as measured by ¹H NMR. In the bulk, the diblock copolymer microphase separates into spherical microdomains of PMMA in a PS matrix. The copolymers were precipitated in methanol and the elemental concentration of residual lithium impurities from the initiator was less than 1 ppm (measured by Quantitative Technologies,

* To whom correspondence should be addressed.

[†] University of Massachusetts.

[‡] Leiden University.

[§] Brookhaven National Laboratory.

Inc) with a 1 ppm resolution.³⁰ The silicon wafer was modified by anchoring a hydroxyl-terminated random copolymer of styrene and methyl methacrylate with a styrene fraction of 0.58 as described previously. Interactions between the PS and PMMA blocks with this modified surface are balanced.³¹ Smooth ~400-nm-thick films of PS-*b*-PMMA were prepared by spin coating 6% (w/v) solutions of the copolymer in toluene onto the modified Si substrate. An aluminized Kapton film comprised the top electrode. A thin layer (20–25 μm) of cross-linked PDMS (Sylgard) was used as a buffer layer between the Kapton electrode and the copolymer thin film to ensure physical contact between the electrode and copolymer film. The copolymer films were heated to 170 °C under N₂ with an applied electric field of ~40 V/μm for 20 h, and then quenched to room temperature before removing the electric field. For transmission electron microscopy, the samples were embedded in epoxy, peeled from the substrate by dipping into liquid N₂, microtomed with a diamond knife at room temperature onto a water surface, and retrieved with a copper grid. The thin sections were exposed to ruthenium tetroxide for 15 min to enhance the contrast. Electron microscopy experiments were performed on a JEOL 200KV TEM at an accelerating voltage of 200 KV. Tapping mode atomic force microscopy (AFM) was performed with a Dimension 3100, Nanoscope III from Digital Instruments Corp. Grazing incidence small-angle X-ray scattering (GISAXS) was performed at the National Synchrotron Light Source, (NLSL, Brookhaven National Laboratory), using X-rays with a wavelength of 1.567 Å. The exposure times were 30 s per sample.

Computer Simulation

Computer simulations of the electric field induced sphere-to-cylinder transition in asymmetric diblock copolymer thin films were done using the simulation software developed at Leiden University on the basis of the dynamic self-consistent field (DSCF) theory.³² Phase separation was monitored by a scalar order parameter $\psi(\mathbf{r}, t)$, which is the normalized deviation of the density of a block copolymer component from its average value. In an incompressible diblock copolymer melt, the system is described by only one order parameter. The chemical potential, in the presence of an electric field \mathbf{E} , has the form $\mu = \mu^0 - (\partial\epsilon/\partial\psi)_T E^2/8\pi^{26}$ where μ^0 is the chemical potential in the absence of the electric field, and ϵ is the dielectric constant of the material, which can be approximated as $\epsilon(\mathbf{r}, t) \approx \epsilon_0 + \epsilon_1\psi(\mathbf{r}, t)$ for small ψ . Because of the inhomogeneity of ϵ , the electric field inside the material \mathbf{E} deviates from the applied electric field $\mathbf{E}_0 = (0, 0, E_0)$ and is $\mathbf{E} = \mathbf{E}_0 - \nabla\varphi$, where the potential φ can be expressed in terms of the order parameter ψ using the Maxwell equation $\text{div}\epsilon\mathbf{E} = 0$. Keeping only leading terms in the divergence of the flux $\nabla^2\mu$, one can write the equation for the time evolution of the order parameter as an anisotropic diffusion equation³³

$$\psi = M\nabla^2\mu^0 + \alpha\nabla_z^2\psi + \eta \quad \alpha \equiv ME_0^2 \frac{\epsilon_1}{4\pi\epsilon_0}$$

with a constant mobility M , and the thermal noise η that is related to the mobility via the fluctuation–dissipation theorem.³² The chemical potential μ^0 is calculated using self-consistent field theory for ideal A_NB_M Gaussian chains with the mean field interactions between copolymer blocks, A and B. The strength of these interactions is described by a parameter ϵ_{AB} , which is related to the Flory–Huggins interaction parameter χ .³² The model system studied here was an A₂B₁₀ melt in a 60³ simulation box (in units of grid spacing h). With the mean field interactions $\epsilon_{AB} = 8$ kJ/

mol, the system gives a spherical microdomain morphology in the absence of an electric field. This simulation box fits about eight microdomains across, as the grid spacing is related to the Gaussian bond length parameter a by $h/a = 0.866$ for numerical considerations.³² The melt is confined between two substrates (electrodes) at $z = -1$ and $z = 61$, with a weak repulsion of the A block ($\epsilon_{AM} = 2.1$ kJ/mol), to mimic experimental conditions.³⁴ The electric field strength is parametrized by $\tilde{\alpha} \equiv \alpha/kTM\nu$ where ν is the bead volume. The M enters the simulations only in combination with time t via a dimensionless time step $\Delta\tau = kTM\nu h^{-2}\Delta t = 0.5$.³² The volume fraction of the minority component, 0.167, is different from the experimental system, however, well within the range of the spherical morphologies, keeping in mind that a specific morphology typically extends over a volume fraction range of about 0.1. The experimental volume fraction of 0.1 would require A₂B₁₈ to be the shortest possible simulation molecule, which is almost twice as long as A₂B₁₀ and requires an exceedingly large computational effort. Any difference in kinetic behavior because of this slight change in the volume fraction is expected to be minimal and a qualitative comparison is certainly possible.

Results and Discussion

To confirm that the copolymer thin films formed spherical microdomains, a ~50-nm film was spin-coated onto a silicon wafer having a native silicon oxide layer and annealed at 170 °C under vacuum for 48 h. The film was then exposed to UV and rinsed with acetic acid to selectively remove the PMMA block.¹⁷ Figure 1a shows the in-plane view AFM phase image. Spherical domains with liquidlike packing can be seen because of the comparable surface tension of PS and PMMA and film thickness constraint.³⁵ The diameter of the PMMA microdomains is ~22 nm with a center-to-center distance of ~41 nm. The surface of films thicker than several equilibrium periods was covered by the PS block, the lower surface energy component, and was featureless. Figure 1b is the cross-sectional TEM image of a ~400-nm film annealed at 170 °C under vacuum for 48 h. A layering of spherical microdomains induced by the substrate (or air)/copolymer interfaces is clearly seen.^{36,37} From this side view, the packing of the spherical microdomains is not well-defined. In Figure 1c, a typical grazing incidence small-angle X-ray scattering pattern taken at an incidence angle of ~0.2° for the same film as in Figure 1b is shown. This incident angle is higher than the critical angle of the polymer and lower than the critical angle of silicon substrate and thus the beam penetrated through the entire film. The ring of scattering confirms the random packing of the spherical microdomains. The nonuniformity in the azimuthal dependence of the scattering arises, more than likely, from the layering of the spherical microdomains induced by the interfaces as shown in Figure 1b. The streak of intensity parallel to the film surface (i.e., in q_y) is a reflection/scattering of the incident beam. The scattering intensity is relatively weak because of the small electron density difference between the PS and PMMA and the low volume fraction of the spherical microdomains (10%). These observations are also consistent with the computer simulation, where the film adjacent to the substrate is the major component B which has the lower surface energy. The spherical domains in the film have a three-dimensional liquidlike packing, Figure 1d. A side view of the simulation box in Figure 1e clearly

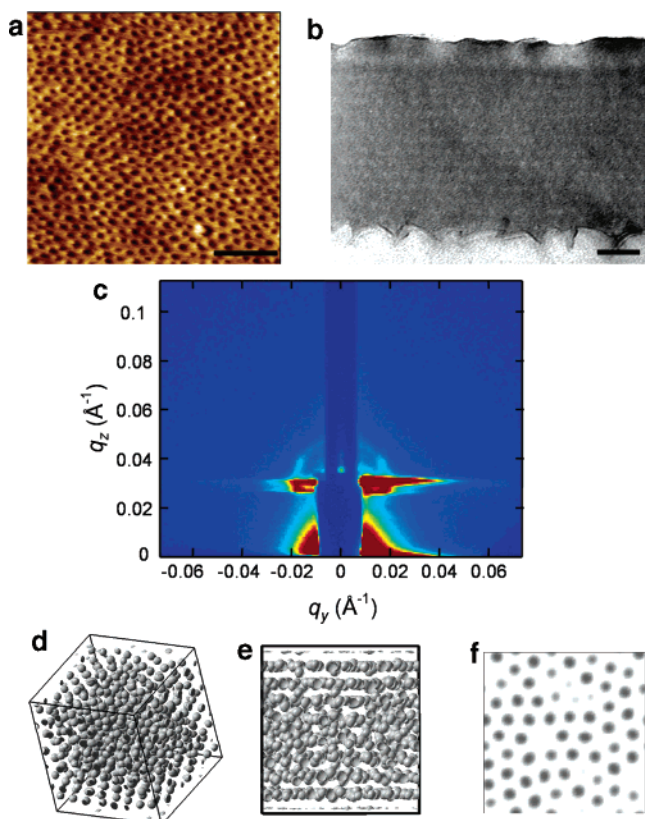


Figure 1. (a) AFM phase image of a ~ 50 -nm PS-*b*-PMMA film annealed 48 h at 170°C under vacuum, then exposed to UV and rinsed with acetic acid. Image size: $1 \times 1 \mu\text{m}^2$. (b) Cross-sectional TEM image of a ~ 400 -nm PS-*b*-PMMA film annealed 48 h at 170°C under vacuum. Scale bar: 100 nm. (c) Grazing incidence small-angle X-ray scattering pattern of a ~ 400 -nm PS-*b*-PMMA film annealed 48 h at 170°C under vacuum. (d) DSCF simulation snapshot of the asymmetric block copolymer melt after 5000 time steps, prior to applying an electric field. The image (and others that follow) shows isodensity surfaces (50% of the maximum concentration) of the minority block. (e) Side view of the simulation snapshot shown in Figure 1d. Two substrates (serving later as electrodes) are present at the top and bottom of the simulation box (not visible in the images). (f) Cross section of the film in Figure 1d at $z = 42$ (parallel to the film surface).

shows surface-induced layering of the spherical microdomains, which is enhanced in the vicinity of the surfaces. The in-plane packing is not well defined and the packing is liquidlike as seen in the top view in Figure 1f.

Figure 2a shows the GISAXS pattern taken at an incidence angle of $\sim 0.2^\circ$ of a ~ 400 -nm film after annealing under a $\sim 40 \text{ V}/\mu\text{m}$ electric field for 24 h. The peaks along q_z , which reflect density correlations normal to the surfaces, are not observed. Thus, interferences normal to the surface, and hence the layered structure of the spherical domains seen initially, have vanished. However, along q_y (in the plane of the film) multiple reflections are evident. This suggests that microdomains are aligned normal to the substrate and are no longer spherical. A q_y scan at $q_z \approx 0.022 \text{ \AA}^{-1}$ is shown in Figure 2b. After annealing under an electric field, a first-order peak is seen at $q \approx 0.0154 \text{ \AA}^{-1}$ and higher order reflections with peak positions relative to the first order are seen at $1:\sqrt{3}:\sqrt{4}:\sqrt{7}:\sqrt{9}:\sqrt{12}$. This indicates that the microdomains oriented normal to the surface are laterally packed into a hexagonal array. A q_y scan from the left side of the GISAXS image in Figure 1c was also

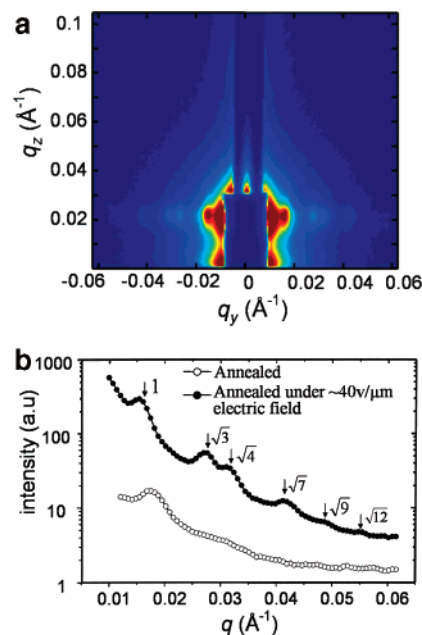


Figure 2. (a) Grazing incidence small-angle X-ray scattering pattern of a ~ 400 -nm PS-*b*-PMMA film annealed at 170°C under a $\sim 40 \text{ V}/\mu\text{m}$ electric field for 24 h. (b) The q_y scan at $q_z \approx 0.022 \text{ \AA}^{-1}$ of the left side of the GISAXS pattern of the films annealed with and without electric field.

plotted for comparison. For the film annealed without electric field, only the first-order peak at $q \approx 0.0174 \text{ \AA}^{-1}$ with a diffuse shoulder is seen suggesting a morphology consistent with disordered arrays of spheres or lattice disordered spheres (LDS) as discussed by Hashimoto et al.^{10,38} The shifting of the first-order peak to a lower q is also consistent with thermoreversible OOT from a disordered sphere to hexagonally packed cylinder morphology instead of simple reorientation of cylindrical microdomains.³⁸ Thus, by applying an electric field normal to the surface, the spherical microdomains were transformed into cylindrical microdomain oriented normal to the surface. However, with GISAXS, it is not possible to discern whether the alignment of the microdomains extends completely to the interfaces.

Figure 3a shows the AFM phase image of a copolymer thin film after annealing under electric field at 170°C under N_2 for ~ 20 h. The fast Fourier transform (FFT) of part of the image is shown in the inset. Hexagonally packed PMMA domains in a PS matrix are seen. After deep UV exposure and rinsing with acetic acid, the AFM image in Figure 3b was obtained showing a nanoporous film with pores ~ 14 nm in diameter. Figure 3c shows the cross-sectional TEM image of the film. The brighter PMMA cylinders oriented normal to the substrate are seen to penetrate through the entire film. The roughness on the surface is due to the fracture separation of the film from the neutral surface after dipping into liquid N_2 . In the computer simulation, application of the electric field above a certain threshold value normal to the film surface transforms the spherical phase in Figure 1d into an array of hexagonally packed cylinders aligned along the field direction shown in Figure 3d. The side view shows that the cylinders penetrate through the entire film with very few defects, Figure 3d. In accordance with the experimental findings, the diameters of the cylinders are smaller than the radii of the initial spheres (compare Figures 3e and 1e). The in-

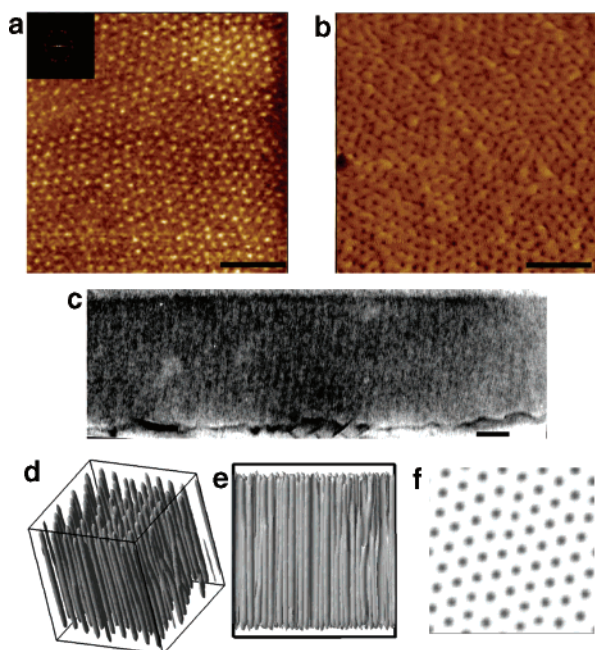


Figure 3. AFM phase image of a ~ 400 -nm PS-*b*-PMMA film annealed at 170°C under a ~ 40 V/ μm electric field for 24 h (a) before and (b) after UV exposure and acetic acid rinsing to remove PMMA blocks. (c) Cross-sectional TEM image of the film. Image size: $1 \times 1 \mu\text{m}^2$. (d) DSCF simulation snapshots of the asymmetric block copolymer melt in the presence of an electric field at 20 000 time steps. The electric field of strength $\tilde{\alpha} = 0.5$ was applied at 16 000 time steps. (e) Side view of the simulation snapshot shown in Figure 3d. (f) Cross section of the film in Figure 3d at $z = 42$ (parallel to the film surface).

plane hexagonal packing contains several long-living structural defects (a total of four in our simulation box), Figure 3e.

The process by which the sphere-to-cylinder transition occurs can be elucidated by the cross-sectional TEM image in Figure 4. This copolymer film has been annealed under electric field for 10 h, shorter than the time necessary to produce the cylindrical microdomains shown in Figure 2. A mixed morphology of undeformed spheres (A, B), deformed spheres (C, D), and interconnected spheres or ellipsoids (E) are seen in one image. On the basis of these different observations, the transition process can be deduced. In the early stage of the alignment, the diblock copolymer forms spherical microdomains even in the presence of electric field. In A, B, the spherical microdomains have not yet been deformed. After annealing under an electric field for a longer time, the spherical microdomains in region A are deformed into ellipsoids (C, D) with their long axes oriented in the direction of the applied electric field. Then, the ellipsoids due most likely to induced polarization charges interconnect (E). These interconnections are not oriented in the field direction but, rather, are dictated by the proximity of poles of the ellipsoids of different sign. Eventually, they interconnect to cylindrical domains that become oriented along the field lines. The same evolution picture can be deduced from snapshots at the initial stage of transformation, Figure 4b, which shows slices of the three-dimensional structure. At the initial stages, a coexistence of deformed spheres, ellipsoids, and short cylinders are seen. Although the model includes only a dielectric mismatch and no charges, the ellipsoids tend to connect at a nonzero angle with the electric field lines, which is solely due to the

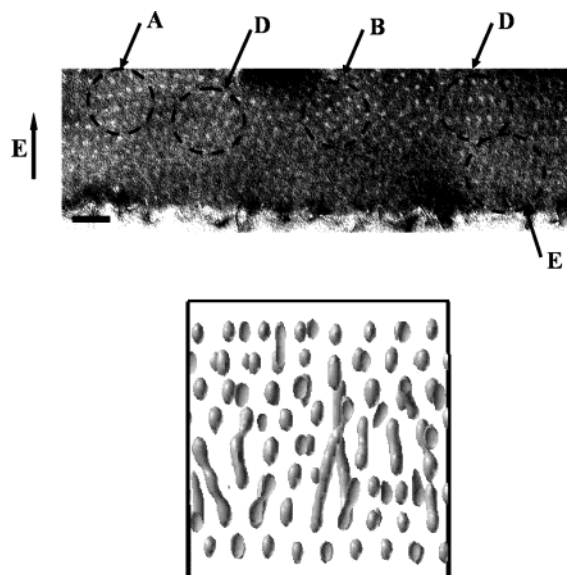


Figure 4. (a) Cross-sectional TEM image of a ~ 400 -nm PS-*b*-PMMA film annealed at 170°C under a ~ 40 V/ μm electric field for ~ 10 h. Different morphologies are discernible. Region A, B: undeformed spherical microdomains. Region C, D: deformed spherical microdomains. Region E: deformed spherical microdomain connected into cylinders. Scale bar: 100 nm. (b) Side view of two slices at different positions in the three-dimensional simulation snapshot at the initial stage (16 075 time steps) of the sphere-to-cylinder transition. The slices are each about one cylinder diameter thick. The electrodes are present at the top and bottom of the simulation box (not visible in the images).

geometric proximity of the ellipsoids. The exact value of the angle may be different if ion impurities would be taken into account.

The electric field induced transition from spherical microdomains to cylinders was theoretically predicted to be ~ 70 V/ μm for the PS/PMMA system on the basis of dielectric constants difference ($\epsilon_{\text{PS}} \approx 2.5$, $\epsilon_{\text{PMMA}} \approx 6$).²⁷ It was argued that presence of the dissociated Li ions in the block copolymer would considerably lower electric field necessary to induce the sphere-to-cylinder transition. Here, the transition occurred at an electric field strength of ~ 40 V/ μm , much lower than the calculated critical field strength based on differences in the dielectric constants of PS and PMMA. This reduced field strength could easily be due to presence of trace lithium ion used in the anionic copolymerization. The elemental concentration of lithium impurities was less than 1 ppm, the best resolution we could achieve. This, however, is much higher than the concentration necessary to reduce the critical electric field strength. Further experiments are underway to quantify the effect of lithium ions on the electric field alignment of diblock copolymer thin films and will be reported at a later date.

The simulation suggests a way to eliminate remaining defects in the hexagonal array of cylinders. By switching the electrical field off, the system in Figure 3d reverts to the spherical microphase separated morphology, however, with improved packing. Switching the electrical field on again leads to a reformation of cylinders, Figure 5, with an in-plane defect density that is significantly lower (two in our simulation box). The process is mediated by the phase transition back to the spherical phase, where eliminating defects is energetically less costly and kinetically easier.

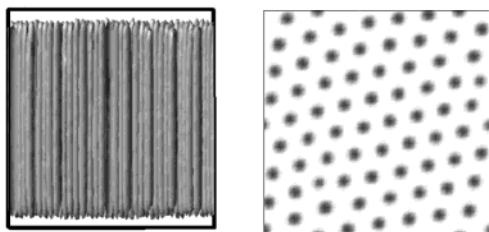


Figure 5. DSCF simulation snapshots of the asymmetric diblock copolymer melt after one more cycle of alternating switching of the electric field (switch off at 20 000 time steps and on again at 30 000 time steps). The simulation snapshot is at 35 000 time steps. (a) Side view of the three-dimensional simulation snapshot. (b) Cross section of the simulation snapshot parallel to the electrodes ($z = 42$).

Conclusion

An electric field induced sphere-to-cylinder transition in PS-*b*-PMMA diblock copolymer thin films has been observed. In the absence of an applied electric field, thin films of the asymmetric diblock copolymer consisted of layers of spherical microdomains with poor in-plane ordering. Under a ~ 40 V/ μm applied electric field, hexagonally packed cylindrical microdomains oriented normal to the surface were found. After selectively remove the minor component, AFM images revealed cylindrical microdomains with diameters smaller than that of the original spherical microdomains. Cross-sectional TEM images of intermediate stages of the alignment indicate that under electric field, the asymmetric diblock copolymer forms the spherical microdomains that are deformed into ellipsoids that, with time, interconnect to form cylindrical microdomains oriented in the direction of the applied electric field. These findings were confirmed by simulations which also suggested that better long-range order of the cylindrical microdomains could be achieved by cycling the electrical field from on to off.

Acknowledgment. This work was funded by Department of Energy, Office of Energy Sciences (DEFG02-96ER45612), the National Science Foundation-supported Material Research Science and Engineering Center (MRSEC) at University of Massachusetts, Amherst (DMR-0213695), and the Army Research Laboratory, Polymer Center of Excellence at the University of Massachusetts, Amherst. Supercomputer time was provided by the Stichting Nationale Computerfaciliteiten (NCF), Amsterdam. This work is supported by U.S. Department of Energy's Nanoscale Science, Engineering, and Technology (NSET) program under contract no. DE-AC0298CH10886.

References and Notes

- Bates, F. S.; Fredrickson, G. H. *Annu. Rev. Phys. Chem.* **1990**, *41*, 5252.
- Park, M.; Harrison, C.; Chaikin, P. M.; Register, R. A.; Adamson, D. *Science* **1997**, *276*, 1401.
- Leibler, L. *Macromolecules* **1980**, *13*, 1602.
- Wang, C. Y.; Lodge, T. P. *Macromolecules* **2002**, *35*, 6997.
- Wang, C. Y.; Lodge, T. P. *Macromol. Rapid Commun.* **2002**, *23*, 49.
- Sakurai, S.; Hashimoto, T.; Fetters, L. J. *Macromolecules* **1996**, *29*, 740.
- Sakamoto, N.; Hashimoto, T.; Han, C. D.; Kim, D.; Vaidya, N. Y. *Macromolecules* **1997**, *30*, 1621.
- Matsen, M. W. *J. Chem. Phys.* **2001**, *114*, 8165.
- Krishnamoorti, R.; Silva, A. S.; Modi, M. A.; Hammouda, B. *Macromolecules* **2000**, *33*, 3803.
- Kimishima, K.; Koga, T.; Hashimoto, T. *Macromolecules* **2000**, *33*, 968.
- Hajduk, D. A.; Gruner, S. M.; Rangarajan, P.; Register, R. A.; Fetters, L. J.; Honeker, C.; Albalak, R. J.; Thomas, E. L. *Macromolecules* **1994**, *27*, 490.
- Ryu, C. Y.; Vigild, M. E.; Lodge, T. P. *Phys. Rev. Lett.* **1998**, *81*, 5354.
- Amundson, K.; Helfand, E.; Davis, D. D.; Quan, X.; Patel, S. S.; Smith, S. D. *Macromolecules* **1991**, *24*, 6546.
- Boker, A.; Knoll, A.; Elbs, H.; Abetz, V.; Muller, A. H. E.; Krausch, G. *Macromolecules* **2002**, *35*, 1319.
- Mansky, P.; DeRouchey, J.; Russell, T. P.; Mays, J.; Pitsikalis, M.; Morkved, T.; Jaeger, H. *Macromolecules* **1998**, *31*, 4399.
- Morkved, T. L.; Lu, M.; Urbas, A. M.; Ehrlich, E. E.; Jaeger, H. M.; Mansky, P.; Russell, T. P. *Science* **1996**, *273*, 931.
- Thurn-Albrecht, T.; Steiner, R.; DeRouchey, J.; Stafford, C. M.; Huang, E.; Bal, M.; Tuominen, M.; Hawker, C. J.; Russell, T. P. *Adv. Mater.* **2000**, *12*, 1138.
- Onuki, A.; Fukuda, J. *Macromolecules* **1995**, *28*, 8788.
- Lin, Z. Q.; Kerle, T.; Baker, S. M.; Hoagland, D. A.; Schaffer, E.; Steiner, U.; Russell, T. P. *J. Chem. Phys.* **2001**, *114*, 2377.
- Schaffer, E.; Thurn-Albrecht, T.; Russell, T. P.; Steiner, U. *Nature* **2000**, *403*, 874.
- Thurn-Albrecht, T.; DeRouchey, J.; Russell, T. P.; Jaeger, H. M. *Macromolecules* **2000**, *33*, 3250.
- Thurn-Albrecht, T.; DeRouchey, J.; Russell, T. P.; Kolb, R. *Macromolecules* **2002**, *35*, 8106.
- Pereira, G. G.; Williams, D. R. M. *Macromolecules* **1999**, *32*, 8115.
- Amundson, K.; Helfand, E.; Quan, X.; Smith, S. D. *Macromolecules* **1993**, *26*, 2698.
- Amundson, K.; Helfand, E.; Quan, X.; Hudson, S. D.; Smith, S. D. *Macromolecules* **1994**, *27*, 6559.
- Landau, L. D.; Lifshitz, E. M. *Electrodynamics of Continuous Media*; Oxford, 1960; Chapter II.
- Tsori, Y.; Tournilhac, F.; Andelman, D.; Leibler, L. *Phys. Rev. Lett.* **2003**, *90*, 145504.
- Segalman, R. A.; Yokoyama, H.; Kramer, E. J. *Adv. Mater.* **2001**, *13*, 1152.
- Register, R. A.; al., e. *Abstracts of the American Physical Society* **2001**.
- The lithium elemental concentration was measured by quantitative technology Inc. Website: <http://www.QTionline.com>.
- Mansky, P.; Liu, Y.; Huang, E.; Russell, T. P.; Hawker, C. *Science* **1997**, *275*, 1458.
- van Vlimmeren, B. A. C. v.; Maurits, N. M.; Zvelindovsky, A. V.; Sevink, G. J. A.; Fraaije, J. G. E. M. *Macromolecules* **1970**, *3*, 646.
- Zvelindovsky, A. V.; Sevink, G. J. A. *Phys. Rev. Lett.* **2003**, *90*, 049601.
- Sevink, G. J. A.; Zvelindovsky, A. V.; von Vlimmeren, B. A. C. v.; Maurits, N. M.; Fraaije, J. G. E. M. *J. Chem. Phys.* **1999**, *109*, 2250.
- Fasolka, M. J.; Banerjee, P.; Mayes, A. M.; Pickett, G.; Balazs, A. C. *Macromolecules* **2000**, *33*, 5702.
- Henke, C. S.; Thomas, E. L.; Fetters, L. J. *J. Mater. Sci.* **1988**, *23*, 1685.
- Yokoyama, H.; Mates, T. E.; Kramer, E. J. *Macromolecules* **2000**, *33*, 1888.
- Sota, N.; Sakamoto, N.; Saijo, K.; Hashimoto, T. *Macromolecules* **2003**, *36*, 4534–4543.

MA049235B